Interaction between the VDAC channel and a polyanionic effector

An electron microscopic study

Carmen A. Mannella and Xiao-Wei Guo

Wadsworth Center for Laboratories and Research, New York State Department of Health, Empire State Plaza, Albany, New York 12201; and Departments of Physics and Biomedical Sciences, State University of New York at Albany, Albany, New York 12201

ABSTRACT The conductance of the voltage-dependent mitochondrial outer membrane channel is modulated by a synthetic anionic polymer. When added to suspensions of membrane crystals of the channel, the polyanion caused disordering of the usual parallelogram array and increased occurrence of a contracted form of the array. Correlation averages obtained from electron microscopic images of the channel crystals indicated a narrowing of the projected channel lumen in the presence of the polyanion and the appearance of new, narrow zones of stain exclusion on the outside of the channel. These effects are interpreted in terms of possible conformational changes induced in the channel by binding of the polyanion.

INTRODUCTION

A prominent 30-kD polypeptide in the mitochondrial outer membrane forms a voltage-dependent ion channel called VDAC or mitochondrial porin (1–3). When inserted in phospholipid bilayers, this large channel (unit conductance 4.5 nS in 1.0 M KCl) switches to lower conductance substates upon application of transmembrane potentials as small as 20 mV (1, 3). Colombini et al. (4) have reported that a copolymer of methacrylate, maleate, and styrene (1:2:3, 10,000 mol wt) induces similar low-conductance states in bilayer-reconstituted VDAC and increases the voltage sensitivity of the channels that remain open. Patch-clamping studies by Tedeschi et al. (5) have shown that this polyanion reduces the ion conductance of mitochondrial outer membranes in a manner consistent with the effects observed with isolated VDAC. There is evidence that mitochondria contain an endogenous protein that similarly alters VDAC permeability and voltage-gating properties (5, 6), raising the possibility that the synthetic polymer is mimicking an endogenous modulator of the outer membrane channel. Such modulation of VDAC permeability may have physiological significance. For example, Benz and co-workers have presented evidence that the polyanion inhibits the transport of adenine nucleotides through the mitochondrial outer membrane, presumably by altering the permeability of the VDAC pore (7).

Electron microscopy and computer image processing is being used to elucidate the structure of the VDAC channel in two-dimensional crystals that are induced in the mitochondrial outer membrane by phospholipase A_2 (8–10). The predominant crystal forms are parallelogram lattices containing six pores per unit cell. Two polymorphs of the parallelogram lattice are commonly observed (Fig. 1), an "oblique" lattice (a = 13 nm, b = 11.5 nm, lattice angle = 109°) and a "contracted" lattice (a = 13 nm, b = 10 nm, angle = 99°). Negative-stain microscopy indicates that little or no protein protrudes from the surface of the membrane crystals. From space-filling considerations, there is room in the unit cell for only one or two 30-kD polypeptides per channel lumen. The mean inner diameter of the VDAC lumen has been estimated at 2.5–3 nm based on averaged projection images of negatively stained crystalline VDAC arrays (11, 12). This value falls in the middle of the range of channel bore estimates inferred from the permeability properties of VDAC, 1.7–4 nm (1, 3, 13, 14). Previous studies with negatively stained crystalline VDAC arrays have led to the localization of cytochrome c binding sites (at phospholipid domains between the hexamer channel complexes [15]) and of clusters of basic amino acids (on the rims of the pores facing inside the hexamer complexes [16]).

At present, nothing is known about the nature of the interaction between VDAC and its polyanionic effector. We have, therefore, applied techniques used in the abovementioned electron microscopic studies to determine whether the polyanion can be localized on projection maps of crystalline VDAC and/or whether the effector induces detectable structural changes in the channels. Such information should help in elucidating the molecular basis for the effects of the polyanion and eventually may shed light on the mechanism of voltage gating of this important channel.

MATERIALS AND METHODS

Specimen preparation

Outer membranes were isolated from mitochondria of the fungus *Neurospora crassa* (FGSC 326) by hypoosmotic lysis and sucrose gradient centrifugation as described previously (8, 17). Crystallization of the channels in these membranes was carried out by the phospholipase A_2/dialysis technique first described by Mannella (10, 17). Five units of bee-venom phospholipase A_2 (Sigma Chemical Co., St. Louis, MO) were added to a 33-ml fraction of freshly isolated mitochondrial outer membranes (~5 μg protein/ml). This dilute membrane suspension was dialyzed overnight in the cold against 200 vol of low-salt buffer (1 mM Tris-HCl, pH 7.5; 0.25 mM EDTA). After dialysis, the membranes were centrifuged (100,000 *g*, 60 min) and resuspended in 100 μl of low-salt buffer, for use in subsequent procedures. Optical diffraction from electron microscopic images of the phospholipase-treated membranes (see below) indicated that a large proportion (~35%) contained well-ordered crystalline arrays of the VDAC channel. The remaining 65% of the membranes in the preparation contained either poorly ordered arrays or no detectable arrays at all.

20-μl aliquots of the phospholipase A_2-treated mitochondrial outer membrane suspension were mixed with equal aliquots of low-salt buffer containing 0 or 10 μM of poly-(methacrylate, maleate, styrene), a generous gift of T. König (Semmelweis University Medical School, Budapest) and M. Colombini (University of Maryland, College Park, MD). After 20 and 60 min, 5-μl aliquots of the membrane suspensions were deposited on carbon/formvar-coated, glow-discharged specimen grids. After 1 min, the grids were blotted with filter paper, washed with low-salt buffer containing 1% aurothioglucose (Sigma Chemical Co.), and air dried.

Electron microscopy and image processing

Electron micrographs were recorded from fields of control and polyanion-containing specimens of Kodak SO163 film (Eastman Kodak, Rochester, NY) with a Philips EM-420T electron microscope operated at 100 kV. Procedures to minimize specimen irradiation were employed, as described earlier (12), resulting in a dose of ~20 electrons/A^2 for each recorded image. Several dozen images were recorded at an instrument magnification of 36,000 from different grids of each of the specimens. The image negatives were scanned with coherent radiation from a He-Ne laser (Jodon Engineering Associates, Ann Arbor, MI) to characterize the membranes in the fields in terms of their crystallinity (see Results). Optical diffraction patterns from crystalline membranes were recorded on Kodak Pan-X or Tech Pan film.

Images of membrane arrays were selected for further processing which contained large (>0.25 μm^2), evenly stained, well-ordered regions (i.e., at least four orders of sharp reflections visible in optical diffraction patterns). Both oblique and contracted polymorphs of the parallelogram VDAC array were included in the analysis. Reciprocal lattice parameters (as determined in the lattice refinement step above) fell within a narrow range of values for each array type (oblique: lattice angle = 108.7 ± 0.7°, a/b = 1.12 ± 0.01; contracted: lattice angle = 99.5 ± 1.3°, a/b = 1.32 ± 0.05). These image fields were digitized with a PDS 1010A flatbed scanning microdensitometer (Perkin-Elmer, Garden Grove, CA) using a scanning grid corresponding to a sampling distance of 0.47 nm.

Averages were made of the crystalline VDAC array images using the SPIDER image processing system (18) implemented on a VAX 11/780 computer (Digital Equipment Corp., Maynard, MA). The averaging procedure (12, 15, 16) involves use of quasi-optical Fourier filtration (19) to provide a preliminary average of each field, which is subsequently used as a reference for correlation analysis (20–22).

A subfield (256 × 256 square pixels) of the array image is padded into a 512 × 512 field and Fourier transformed. A lattice-refinement procedure is used to construct a mask which passes only those Fourier coefficients associated with the reciprocal lattice of one array. (Because the membrane crystals are usually present as collapsed vesicles, it is common for the crystalline areas to contain two overlapped arrays. Provided maxima from the two different lattices do not overlap, the two arrays may be filtered independently.) Inverse transformation of the masked transform yields the projection image of one layer of the channel array.

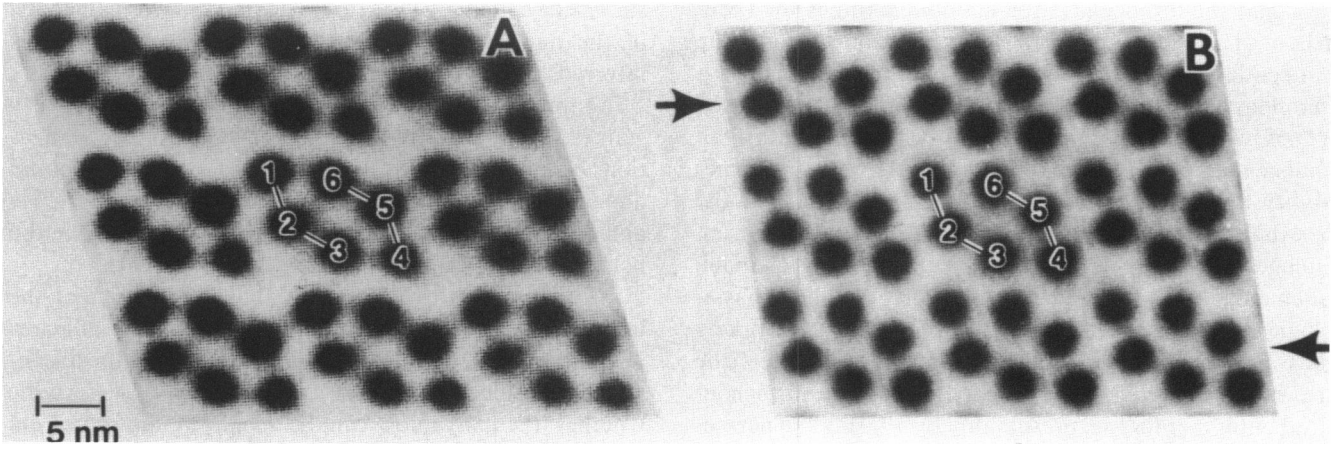

FIGURE 1 Polymorphic forms of the parallelogram VDAC array: (*A*) oblique array; (*B*) contracted array. The unit cell contains six circular negative-stain–filled (dark) pores. The repeating unit may be considered the central group of six channels ("hexamer") in each array. The lattice angle in the oblique array (*A*) is 109°. In the contracted array (*B*), the rows above and below the central row are displaced 1.0 nm in opposite directions (indicated by the arrows), resulting in a new lattice angle of 99°. Also, each row in the "contracted" array is ~1.0 nm narrower (vertical direction) than in the "oblique" array. Note that the arrays in this figure are related by mirroring to those in subsequent figures. Bar, 5 nm. (Figure adapted from Mannella et al. [9].)

A 64 × 64 area is selected from the filtered field, containing a central unit cell (channel hexamer) surrounded by about one-half unit cell in each direction. This reference is cross-correlated with the entire unfiltered field (both padded into a 512 × 512 matrix). The resulting cross-correlation function contains peaks at locations in the raw image where there is a strong match with the reference. A peak-search program is applied to the cross-correlation function to determine the precise coordinates of the centers of gravity of these maxima (23), which are stored in a peak file in order of peak height. Spurious (obviously off-lattice) maxima are deleted from the peak file after visual inspection of point maps generated with the coordinates in this file. The final "correlation average" is formed by addition of 64 × 64 areas extracted from the raw image at the extract positions in the peak file, using bilinear interpolation.

Employing the above procedure, correlation averages were successfully calculated for 9 images of control VDAC arrays and 11 images of polyanion-treated arrays, each representing an average over 120–300 unit cells. Next, bilinear interpolation was used to increase the linear dimensions of the correlation averages (to improve the accuracy of subsequent alignment steps) and to correct the dimensions for slight differences in magnification (based on refined lattice parameters). Each correlation average (now 128 × 128) was centered precisely on the phase origin (diad axis) at the middle of the channel hexamer (located by cross-correlating the average with itself after 180° rotation). Each average was then added to its 180°-rotated version (to enforce p2 symmetry) and rotationally aligned to a common reference by orientation of their respective autocorrelation functions. To co-align correlation averages of oblique and contracted VDAC arrays (for subsequent multivariate statistical analysis), the central unit cell containing a single pore hexamer was masked out before auto-correlation.

A form of multivariate statistical analysis called correspondence analysis was applied to the data set (12, 24). Briefly, each image average containing p pixels after masking is represented as a p-dimensional vector whose component in each ith dimension has a length proportional to the optical density of the ith pixel. The set of 20 aligned image averages thus forms a "cloud" of points defined in p-space by these image vectors. Correspondence analysis determines the orthogonal directions (factor axes) in p-space along which variance in the image cloud is greatest (i.e., along which significant systematic differences occur). The analysis was used in the current investigation to determine whether particular experimental conditions (e.g., presence or absence of polyanion) correlate with systematic changes in the images.

RESULTS

Effect of the polyanion on lattice order and geometry

An electron microscopic image of a typical field of phospholipase A_2-treated, aurothioglucose-embedded mitochondrial outer membranes is presented in Fig. 2. The membranes in this particular field were incubated with the synthetic anionic polymer that is known to modulate VDAC gating characteristics (4, 5, 7).

As noted in the Introduction, the crystalline arrays of VDAC channels observed in these mitochondrial outer membrane suspensions are polymorphic. The most common crystal forms are parallelogram arrays with lattice angles of 109° ("oblique") or 99° ("contracted"). In the phospholipase A_2-treated mitochondrial outer membrane fraction used in the present study, 21% of the arrays were oblique and 14% contracted, before incubation with the polyanion.

Addition of the VDAC-modulating polymer to mitochondrial outer membranes had a dramatic effect on the relative distribution of membrane crystal forms. With increased incubation times, the number of recognizable oblique arrays (determined on the basis of optical diffraction patterns recorded from the image negatives) decreased significantly, dropping from 21% to 6% of the total membrane population after 60 min. This effect appeared to correlate with a rapid and progressive increase in lattice disorder in the oblique arrays, manifest as blurring and splitting of maxima in optical diffraction patterns (not shown). The disordering is visualized more directly in maps of unit cell positions obtained by cross-correlating array images with references composed of a few unit cells (see Materials and Methods). Fig. 3 shows typical lattice maps for negatively stained VDAC arrays in the absence and presence of the polyanionic modulator. The control array is composed of a single, well-ordered lattice, while the polyanion-treated arrays tend to be fragmented. When the maps in Fig. 3 are viewed obliquely, it can be seen that the lattice lines in the modulator-treated arrays are considerably less straight and contain many more dislocations than those in the control arrays. (The disordering effect of the polyanion was first observed with VDAC membrane crystals embedded in uranyl acetate [25]. Because of concerns regarding possible interactions between the polyanion and charged complex ions present in uranyl acetate solution [26], the experiments were repeated in the current study with the uncharged gold-glucose. The latter embedding medium also provides a more native environment for biological molecules, similar to glucose [27].)

By contrast, the polyanion did not have a significant disordering effect on the contracted VDAC arrays in the same fields. In fact, the proportion of contracted arrays increased from 14% to 29% of the total membranes present after 60 min incubation with the polyanion. The concomitant disappearance of the oblique arrays suggests that these arrays are being converted to the contracted polymorph, i.e., that a lateral phase transition is induced by polyanion.

Effects of the polyanion on projection images of the oblique array

Out of several dozen micrographs recorded from fields of control and polyanion-treated mitochondrial outer membranes, 20 images of evenly stained VDAC arrays were found which were sufficiently large and well-ordered to use with the averaging procedures described in Materials and Methods. (It proved to be especially difficult to find

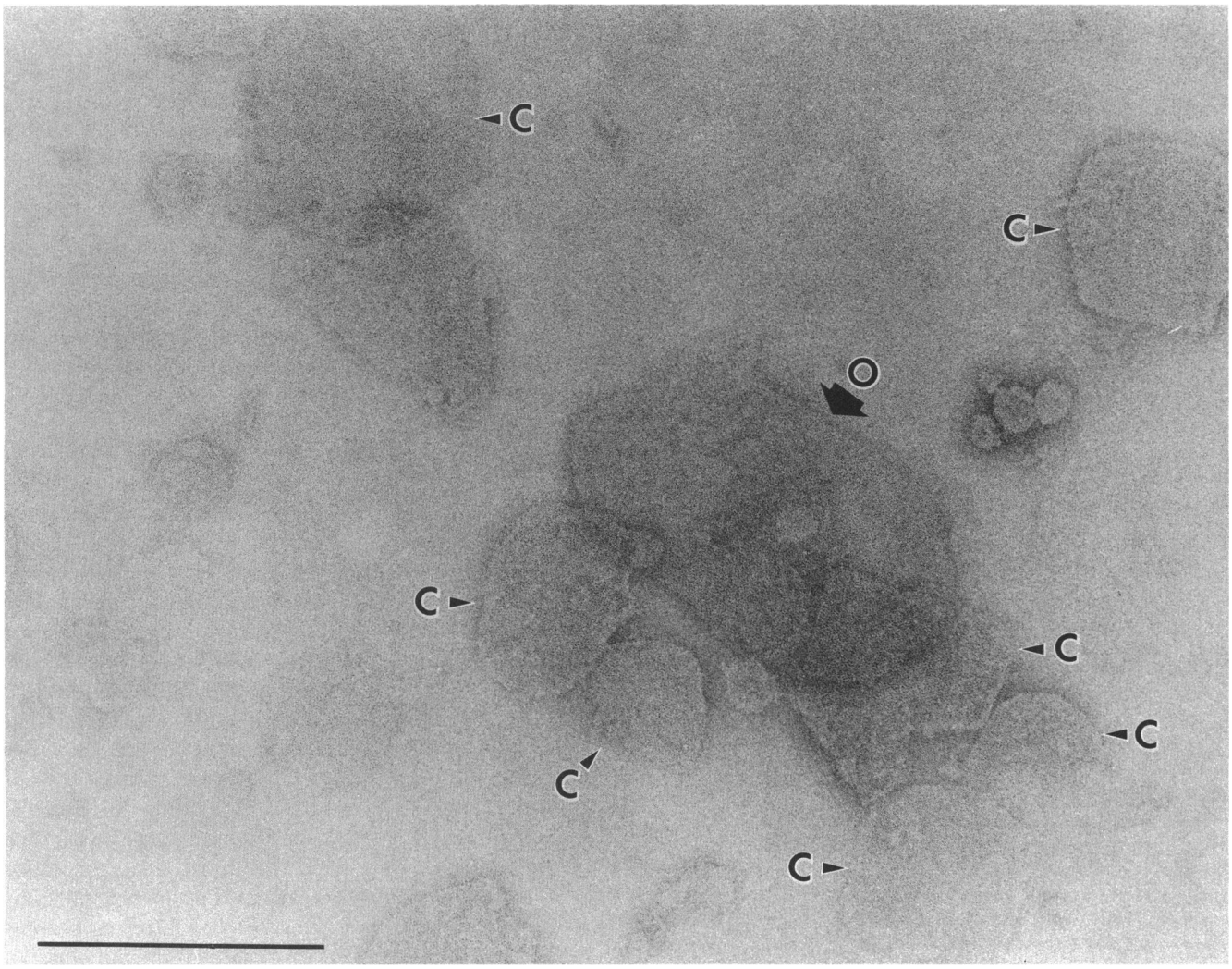

FIGURE 2 Electron micrograph of a field of mitochondrial outer membranes, pretreated with the polyanion and embedded in aurothioglucose. Arrows point to membranes containing periodic VDAC arrays, based on optical diffraction (*O*, oblique lattice; *C*, contracted lattice). The large arrow indicates an array included in the analysis described in the text. Bar, 0.25 μm.

such oblique arrays in the long-term, polyanion-treated specimens.) The correlation averages of these VDAC arrays are presented in the gallery of Fig. 4. These individual averages were summed for each array type (oblique and contracted) to form "specimen averages" (Fig. 5) corresponding to (*A, D*) control, (*B, E*) 20-min polyanion treatment, and (*C, F*) 60-min polyanion treatment. (Each correlation average was scaled to unit mean density before this summation.)

The most obvious effect of polyanion treatment on the VDAC arrays is a decrease in diameter of the stain centers, which represent the axial projections of the stain-filled channel lumens (28). This decrease in projected pore diameter, from ~2.5 to 1.7 nm, is evident in both the individual correlation averages of Fig. 4 and in the specimen averages of Fig. 5.

Statistical corroboration of the link between polyanion treatment and VDAC pore projection diameter was provided by correspondence analysis of the average images of Fig. 4 (12, 24). The first (i.e., most significant) factor axis in the analysis was found to be associated primarily with size of the stain center (total variance associated with Factor 1 = 19%). Fig. 6 is a plot of the position of each image average along Factor 1, organized in rows according to experimental condition (i.e., control, short-term, and long-term exposure to the polyanion). Despite the large spread in these "eigenvalues," especially in the control images, there is a clear demarcation: all 9 control

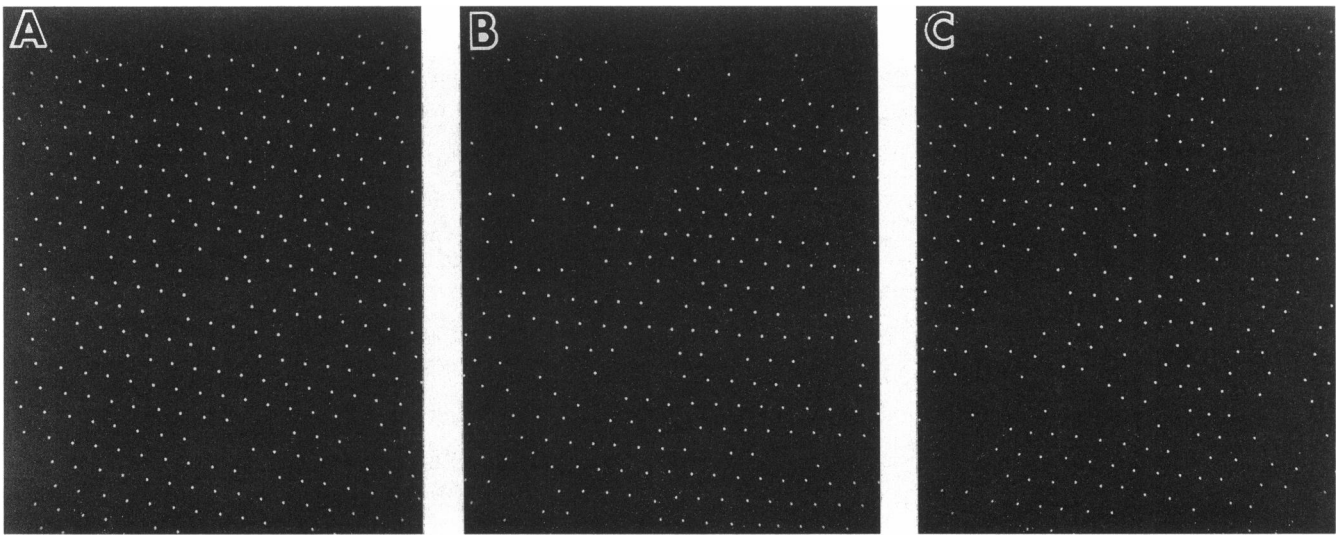

FIGURE 3 Maps of positions of unit cells in oblique VDAC arrays (uranyl acetate-stained), obtained by cross-correlation analysis described in the text. (*A*) Control array. (*B, C*) Arrays treated with the polyanion modulator. Note the increased lattice disorder in *B* and *C*.

images have eigenvalues below 0.05, whereas all but one of the 11 images of polyanion-treated VDAC arrays have eigenvalues $\geq$0.04. It is further evident from Fig. 6 that this effect of the polyanion on VDAC images varies with extent of treatment, i.e., longer exposure correlates with smaller pore diameters (larger eigenvalues). Most of the images of arrays treated for 20 min fall in the eigenvalue range 0.04–0.14, whereas most of the images of arrays treated for 60 min fall in the range 0.15–0.22. Thus, correspondence analysis provides clear evidence for a systematic effect of the polyanion on stain-center diameters in the VDAC arrays.

Another change induced by the polyanion modulator in the VDAC correlation averages are narrow zones of low density (white) that wind around the stain centers. These are evident in the specimen averages (Fig. 5, *C* and *F*) as well as in individual correlation averages (Fig. 4, 8–12, and 16–20). These sinuous stain-excluding features are most often observed in images of long-term, polyanion-treated arrays and never in those of controls.

DISCUSSION

The narrow zones of stain exclusion that appear in correlation averages of VDAC arrays after incubation with the polyanionic modulator (Fig. 5, *C* and *F*) indicate the presence of new material on one or both of the array surfaces. Since these sinuous features are not seen in controls, they most likely represent prominent sites of polyanion binding on crystalline VDAC.

In Fig. 7 *B*, the putative polyanion binding sites of Fig. 5 *C* are superimposed on the correlation average of an unstained, frozen-hydrated oblique array of VDAC (29). In the unmodified map of the projected density of crystalline VDAC (Fig. 7 *A*), protein is black (high density) and the circular, water-filled pores are white (low density). The new elongated white features in Fig. 7 *B* are the strongest stain-excluding regions associated with polyanion binding. The distribution of polyanion around the channel lumens is markedly asymmetric. Moreover, binding occurs primarily along the exterior of the channels, in the region outside the hexamer complex, indicating a preference of the polyanion for the protein/lipid boundary. This partitioning may be explained by the amphiphilic nature of the polyanion, which contains both strongly hydrophobic (styrene) and polar (maleate) residues.

There are several mechanisms by which binding of the polyanion along the outside of the channels might cause the observed lateral phase transition from the oblique to contracted VDAC array. Alterations in protein–lipid and protein–protein interactions are conceivable which might favor one mode of channel packing over another. Another possibility is that the oblique-to-contracted transition is associated with a conformational change in the channel which is itself induced by binding of the polyanion.

The decreased stain accumulation in crystalline VDAC channels induced by polyanion also might be explained by a conformational change, in particular, one which causes a narrowing of the channel lumen. (Note that this conformational change would be distinct from one that might be

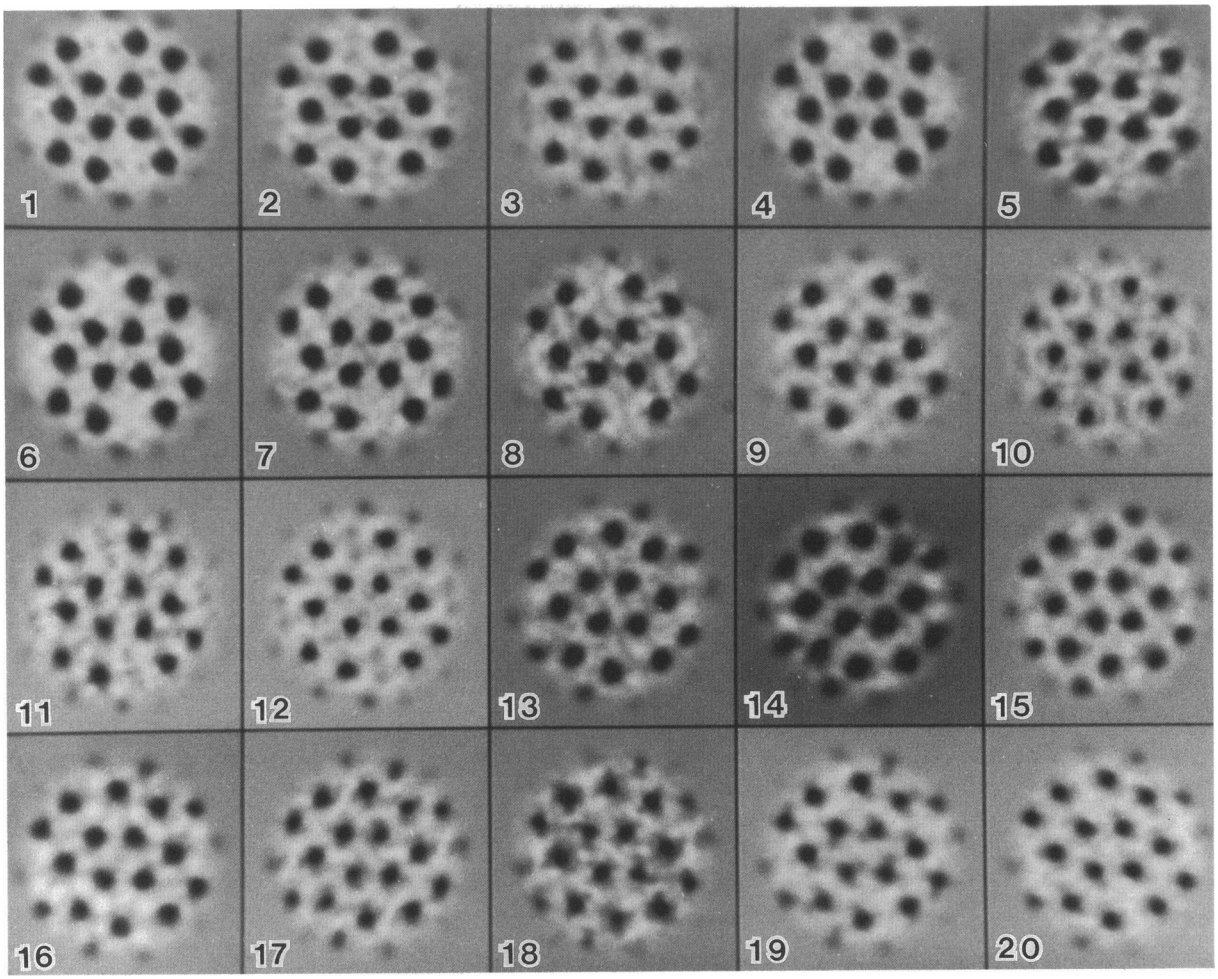

FIGURE 4 Correlation averages of aurothioglucose-embedded VDAC arrays included in the present analysis. (*1–6*) Oblique, control. (*7–9*) Oblique, 20-min polyanion treatment. (*10–12*) Oblique, 60-min polyanion treatment. (*13–15*) Contracted, control. (*16–17*) Contracted, 20-min polyanion treatment. (*18–20*) Contracted 60-min polyanion treatment. Each average is low-pass filtered to 1/(1.7 nm).

associated with crystal phase transitions, since the pores in both oblique and contracted arrays narrow with polyanion exposure.)

Functional studies also suggest that a conformational change is induced in VDAC by the polyanion and that the new conformation is very similar, if not identical, to that associated with voltage-induced closure. Interestingly, the decrease in unit conductance induced by the polyanion or by applied membrane potentials (44%, [1, 4, 7]) is close to the decrease in projected lumen area between control and polyanion-treated arrays in Fig. 5 (54%). However, decreased stain accumulation inside the pores would also result if the polyanion bound to the inside of the pores, thereby excluding the molecules of aurothioglucose.

In summary, the results of the present study indicate that the synthetic polymeric VDAC modulator has several complex effects on the structure of the channel in crystalline arrays. Two of the effects (lateral phase transitions, decreased pore projections) strongly suggest, but do not themselves prove, that the modulator may trigger one or more conformational changes in the channel. Experiments are being undertaken to address this issue directly. A third structural change, the appearance of new stain-excluding regions in the projections of polyanion-treated arrays, probably represents the sites of modulator binding. It should be feasible to determine whether the modulator binds to one or both sides of the channels by three-dimensional reconstruction of the arrays (obtained by combining projections from tilted specimens [30]). If, for example, the polyanion accumulates on only one side of the membrane, it might establish a significant Donnan

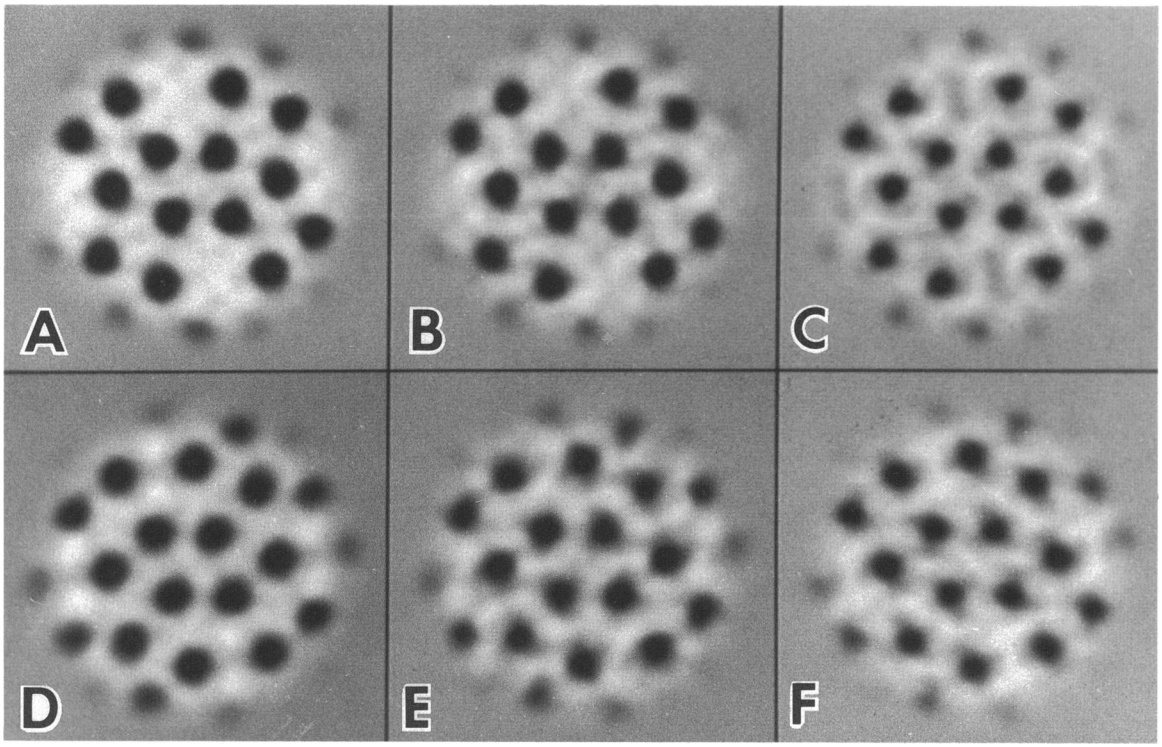

FIGURE 5 Specimen averages of VDAC arrays formed by summing the correlation averages in Fig. 4. (*A*) Oblique, control. (*B*) Oblique 20-min polyanion treatment. (*C*) Oblique 60-min polyanion treatment. (*D*) Contracted, control. (*E*) Contracted, 20-min polyanion treatment. (*F*) Contracted, 60-min polyanion treatment.

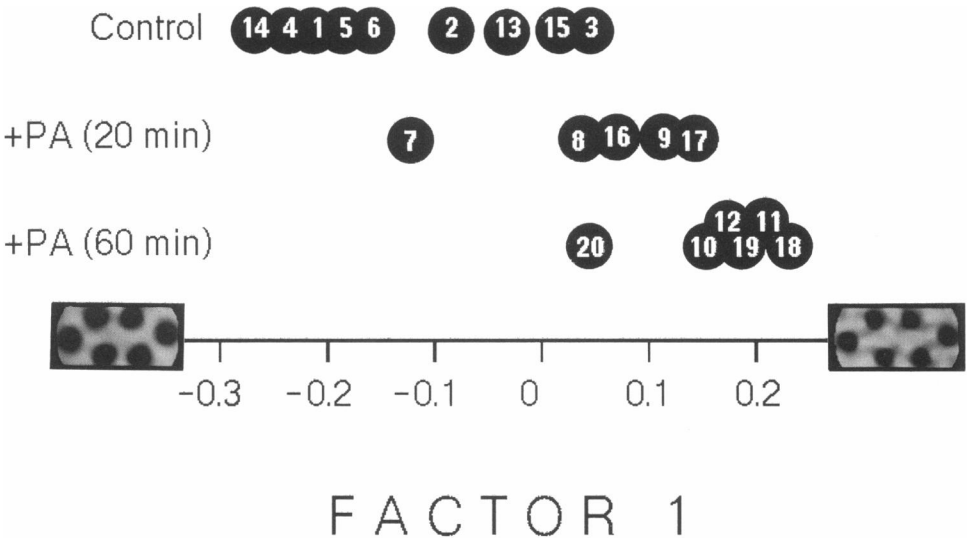

FIGURE 6 Distribution of each correlation average of Fig. 4 along the first factorial direction of the correspondence analysis, described in text. At each end of the Factor 1 axis is an image showing the extreme represented by that direction in image space. Circled numbers correspond to numbering system used in Fig. 4.

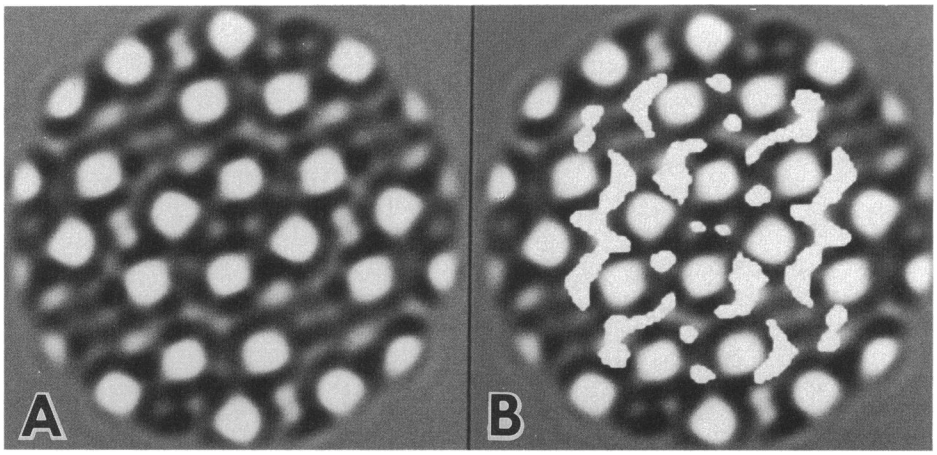

FIGURE 7 Mapping of the putative polyanion binding regions to an unstained, ice-embedded, oblique VDAC array. (*A*) Correlation average of a frozen-hydrated VDAC array, obtained by cryo-electron microscopy; adapted from Mannella et al. (30). Protein is dark and the six circular water-filled pores in each hexameric group are white. (*B*) Superimposition on *A* of the most strongly stain-excluding regions of Fig. 5 *C*. These irregularly shaped, white features probably represent the major sites of polyanion binding to the array surface (see text).

potential. This polyanion-associated field could asymmetrically alter VDAC's sensitivity to applied voltages (depending on their polarity), and might even be large enough to close the channels in the absence of other applied fields, both observed effects (4, 7).

The authors thank Mr. Bernard Cognon for expert technical assistance and Drs. Colombini and J. Frank for several very helpful discussions in the course of these experiments.

This study was supported by National Science Foundation grants PCM-8313045 and DMB-8613702.

Received for publication 10 April 1989 and in final form 28 August 1989.

REFERENCES

1. Colombini, M. 1979. A candidate for the permeability pathway of the outer mitochondrial membrane. *Nature (Lond.).* 279:643–645.
2. Zalman, L. S., H. Nikaido, and Y. Kagawa. 1980. Mitochondrial outer membrane contains a protein producing nonspecific diffusion channels. *J. Biol. Chem.* 255:1771–1774.
3. Benz, R. 1985. Porin from bacterial and mitochondrial outer membranes. *CRC Crit. Rev. Biochem.* 19:145–190.
4. Colombini, M., C. L. Yeung, J. Tung, and T. König. 1987. The mitochondrial outer membrane channel, VDAC, is regulated by a synthetic polyanion. *Biochim. Biophys. Acta.* 905:279–286.
5. Tedeschi, H., C. A. Mannella, and C. L. Bowman. 1987. Patch clamping of the outer mitochondrial membrane. *J. Membr. Biol.* 97: 21–29.
6. Holden, M. J., and M. Colombini. 1988. The mitochondrial outer membrane channel, VDAC, is modulated by a soluble protein. *FEBS (Fed. Eur. Biochem. Soc.) Lett.* 241:105–109.
7. Benz, R., L. Wojtczak, W. Bosch, and D. Brdiczka. 1988. Inhibition of adenine nucleotide transport through the mitochondrial porin by a synthetic polyanion. *FEBS (Fed. Eur. Biochem. Soc.) Lett.* 231:75–80.
8. Mannella, C. A. 1982. Structure of the outer mitochondrial membrane: ordered arrays of porelike subunits in outer-membrane fractions from Neurospora crassa mitochondria. *J. Cell Biol.* 94:680–687.
9. Mannella, C. A., M. Colombini, and J. Frank. 1983. Structural and functional evidence for multiple channel complexes in the outer membrane of Neurospora crassa mitochondria. *Proc. Natl. Acad. Sci. USA.* 80:2243–2247.
10. Mannella, C. A. 1984. Phospholipase-induced crystallization of channels in mitochondrial outer membranes. *Science (Wash. DC.).* 224:165–166.
11. Mannella, C. A., and J. Frank. 1984. Negative staining characteristics of arrays of mitochondrial pore protein: use of correspondence analysis to classify different staining patterns. *Ultramicroscopy.* 13:93–102.
12. Mannella, C. A., A. Ribeiro, and J. Frank. 1986. Structure of the channels in the outer mitochondrial membrane. Electron microscopic studies of the periodic arrays induced by phospholipase A_2 treatment of the Neurospora membrane. *Biophys. J.* 49:307–318.
13. Colombini, M. 1980. Structure and mode of action of a voltage dependent anion-selective channel (VDAC) located in the outer mitochondrial membrane. *Ann. NY Acad. Sci.* 341:552–563.
14. DePinto, V., O. Ludwig, J. Krause, R. Benz, and F. Palmieri. 1987. Porin pores of mitochondrial outer membranes from high and low eukaryotic cells: biochemical and biophysical characterization. *Biochim. Biophys. Acta.* 894:109–119.
15. Mannella, C. A., A. Ribeiro, and J. Frank. 1987. Cytochrome *c* binds to lipid domains in arrays of mitochondrial outer membrane channels. *Biophys. J.* 51:221–226.
16. Mannella, C. A., and J. Frank. 1987. Effects of succinylation on images of negatively stained arrays of mitochondrial outer membrane channels. *J. Ultrastruct. Mol. Struct. Res.* 86:31–40.

17. Mannella, C. A. 1986. Mitochondrial outer membrane channel (VDAC, porin) two-dimensional crystals from Neurospora. *Methods Enzymol.* 125:595–610.

18. Frank, J., B. Shimkin, and H. Dowse. 1981. SPIDER: a modular software system for electron image processing. *Ultramicroscopy.* 6:343–358.

19. Goldfarb, W., J. Frank, M. Kessel, J. C. Jsung, C. H. Kim, and T. E. King. 1979. Cytochrome oxidase vesicles with two-dimensional order. *In* Cytochrome Oxidase. T. E. King, Y. Orii, B. Chance, and K. Okunuki, editors. Elsevier Biomedical Press, Amsterdam. 161–175.

20. Saxton, W. O. 1980. Matching and averaging over fragmented lattices. *In* Electron Microscopy at Molecular Dimensions. W. Baumeister and W. Vogell, editors. Springer-Verlag GmbH and Co., KG, Berlin. 244–255.

21. Frank, J. 1982. New methods for averaging nonperiodic objects and distorted crystals in biologic electron microscopy. *Optik.* (Stuttgart). 63: 67–89.

22. Kessel, M., M. Radermacher, and J. Frank. 1985. The structure of the stalk surface of a brine pond microorganism: correlation averaging applied to a double layered lattice structure. *J. Microsc. (Oxf.).* 139:63–74.

23. Saxton, W. O., and W. Baumeister. 1982. The correlation averaging of a regularly arranged bacterial cell envelope protein. *J. Microsc. (Oxf.).* 127:127–138.

24. Frank, J., A. Verschoor, and M. Boublik. 1982. Multivariate statistical analysis of ribosome electron micrographs. L and R lateral views of the 40S subunit from HeLa cells. *J. Mol. Biol.* 161:107–137.

25. Mannella, C. A., and J. Frank. 1987. Differences in electron microscopic images of the mitochondrial channel, VDAC, caused by its effectors. *Biophys. J.* 51:230*a*. (Abstr.)

26. Tzaphlidou, M., J. A. Chapman, and M. H. Al-Samman. 1982. A study of positive staining for electron microscopy using collagen as a model system. II. Staining by uranyl ions. *Micron.* 13:133–145.

27. Kuhlbrandt, W. 1982. Discrimination of protein and nucleic acids by electron microscopy using contrast variation. *Ultramicroscopy.* 7:221–232.

28. Mannella, C. A., M. Radermacher, and J. Frank. 1984. Three-dimensional structure of mitochondrial outer-membrane channels from fungus and liver. *In* Proceedings 42nd Annual Meeting Electron Microsc. Society of America. G. W. Bailey, editor. San Francisco Press, San Francisco. 644–645.

29. Mannella, C. A., X. Guo, and B. Cognon. 1989. Diameter of the mitochondrial outer membrane channel: evidence from electron microscopy of frozen-hydrated membrane crystals. *FEBS (Fed. Eur. Biochem. Soc.) Lett.* 253:231–234.

30. Amos, L. A., R. Henderson, and P. N. T. Unwin. 1982. Three-dimensional structural determination by electron microscopy of two-dimensional crystals. *Prog. Biophys. Mol. Biol.* 39:183–231.